JOURNAL OF GEOPHYSICAL RESEARCH, VOL. 112, A05207, doi:10.1029/2006JA012001, 2007

High-resolution multifluid simulations of the plasma environment near the Martian magnetic anomalies

E. M. Harnett[1] and R. M. Winglee[1]

Received 2 August 2006; revised 19 December 2006; accepted 23 January 2007; published 12 May 2007.

[1] Three-dimensional high-resolution (~40 km), multifluid simulations of the solar wind interaction at Mars during the southern hemisphere summer solstice indicate that the region around the magnetic anomalies can be complex and highly structured. The anomalous magnetic field leads to the formation of multiple cusps and a void region where the ionosphere is eroded. Most importantly, the anomalous magnetic field changes the nature of the magnetic pileup layer (MPL) when compared to over unmagnetized regions. While the altitude of the MPL is approximately the same in both the northern and southern hemispheres for this orientation, plasma in the MPL near the magnetic anomalies is cooler, with less solar wind and more of ionospheric origin. The solar wind density is reduced by a factor of 3 in the southern MPL, in comparison to the northern MPL, while the ionospheric density is 10–600 times more dense in the southern MPL, depending on altitude, location, and species.

Citation: Harnett, E. M., and R. M. Winglee (2007), High-resolution multifluid simulations of the plasma environment near the Martian magnetic anomalies, *J. Geophys. Res.*, *112*, A05207, doi:10.1029/2006JA012001.

1. Introduction

[2] Mars does not currently possess a global magnetic field but the atmosphere and ionosphere present enough of an obstacle that a bow shock forms, with an average subsolar distance of $1.7R_M$ [*Vignes et al.*, 2000]. As the interplanetary magnetic field (IMF) meets a high conductivity planetary plasma, the IMF begins to pile up, forming a magnetic pileup boundary (MPB). An MPB exists near any nonmagnetized, comet-like object which has a dense and extended atmosphere/ionosphere [e.g., *Mazelle et al.*, 1989]. At Mars, the MPB is also a region where solar wind ions undergo charge exchange with exospheric neutrals [*Riedler et al.*, 1989] and solar wind electrons rapidly lose energy through impact ionization with exospheric neutrals [*Crider et al.*, 2000]. The transition from outside the MPB to inside appears as a large increase in the magnitude of the magnetic field, a decrease in the magnetic field fluctuations, and a simultaneous sharp decrease in the high-energy (solar wind) electron flux [*Vignes et al.*, 2000], as solar wind electrons begin ionizing planetary hydrogen and oxygen [*Crider et al.*, 2000].

[3] The strong southern magnetic anomalies [*Acuna et al.*, 1999; *Connerney et al.*, 1999] are not strong enough or wide-scale enough to lead to the formation of a global magnetopause but still exert a significant influence on the near space plasma. While the anomalies do not appear to modify the location or shape of the bow shock [*Vignes et al.*, 2002], *Crider et al.* [2002] found that the location of the MPB shows both latitudinal and longitudinal dependence, as a result of the presence of the magnetic anomalies. *Crider et al.* [2002] found the average subsolar distance of the MPB to be $1.4R_M$ with the average altitude on the dayside southern hemisphere 200 km (or $0.06R_M$) higher than the dayside northern hemisphere. However, the average MPB altitude increased with increasing latitude in the southern hemisphere and was also found to be highly variable. Also, *Brain et al.* [2005] found that not only is the sheath typically at a higher altitude in the southern hemisphere, the altitude of formation also depends on IMF orientation and season.

[4] Besides increasing the altitude of the formation of the MPB, the anomalous magnetic field can also interact with the IMF to form cusp-like structures. Looking at Mars Global Surveyor (MGS) data from the nightside, *Mitchell et al.* [2001] found regions of flux spikes consisting of sheath-like electron populations that separated void regions of reduced plasma flux. The features, named magnetocylinders, are like the Earth's cusp in that the flux spikes occurred in the vicinity of strongly radia l magnetic field, but, unlike the Earth's cusps, have a linear extent of thousands of kilometers. A statistical analysis of MGS data from the dayside by *Brain et al.* [2005] indicated that in general, sheath-like plasma was detected at 400 km in the northern hemisphere on the order of 20% of the time and 0–5% of the time in the southern hemipshere. However, over two cusp-like regions of strongly radial magnetic field in the southern hemisphere, sheath-like plasma was detected on the order of 15% of the time. Cusp-like features with sheath-like electron populations have also been seen in Mars Express (MEX) measurements [*Soobiah et al.*, 2006; *Franz et al.*, 2006]. In addition, there is evidence of solar wind penetration down to ~300 km in some regions [*Lundin et al.*, 2004, 2006].

[1]Department of Earth and Space Sciences, University of Washington, Seattle, Washington, USA.

0148-0227/07/2006JA012001$09.00

[5] Three-dimensional (3-D) ideal MHD simulations of the Martian magnetosphere, using a magnetized Mars, were conducted by *Ma et al.* [2002] to investigate the effects of the hot oxygen corona on the locations of the ionopause and bow shock. They found that the position of the ionopause was approximately 100 km further from the surface over the southern hemisphere than the northern hemisphere due to the anomalous magnetic field. The model also showed the formation of a magnetocylinder type structure on the nightside. However, their model could not resolve the magnetic pileup boundary and thus did not make any predictions about the affect of the anomalies on this boundary.

[6] Previous 3-D single fluid simulations of the solar wind interaction with Mars [*Harnett and Winglee*, 2003] suggested that a minimagnetopause forms in place of the MPB in the southern hemisphere when the strongest magnetic anomalies are on the day side. The nonideal MHD nature of the model meant it could capture the particle type effects occurring within the magnetosphere and resolve the MPB. The results suggested that the signature for crossing a minimagnetopause would be very similar to crossing the MPB. However, these results were for a single fluid model and the grid space was also such that the some features were only barely resolved.

[7] This paper presents results from high-resolution, 3-D multifluid simulations of the solar wind interaction with the anomalous magnetic field at Mars. In addition to capturing the difference in light and heavy ion dynamics (unlike MHD simulations), the order of magnitude improvement in resolution by means of a high-resolution gridding means that small-scale structures around the magnetic anomalies can begin to be resolved within the context of a global model (unlike hybrid simulations). Distinguishing between solar wind and ionospheric populations with high resolution, allows for a better understanding of how the anomalous magnetic field modifies both the local solar wind-ionosphere interaction and the role it plays in global plasma/magnetic field interactions. Comparison of the results with data allows for the development of a global picture that is difficult to determine from satellite data alone.

2. Model

[8] The multifluid model [*Winglee*, 2004] can assume any number of ion species, only limited by computational speed. In the results presented in this paper, three ion species were assumed: an H^+ solar wind and a planetary ionosphere composed of H^+ and O_2^+. Viking 1 measured O_2^+ to be the primary heavy ion below about 300 km, with a density of $\sim 10^3$ cm^{-3} at 250 km, reaching a maximum density of 10^5 cm^{-3} at 130 km from the surface [*Hanson et al.*, 1977]. O_2^+ is used in these simulations to represent heavy ions. Ionospheric hydrogen is also included to investigate the difference between light and heavy ions of planetary origin. The inner boundary is defined as 250 km above the surface with the number densities of 200 O_2^+ cm^{-3} and 50 H^+ cm^{-3} at the equator. Higher densities at the inner boundary generated unrealistic outflows as the model does not include all possible loss mechanisms such as those due to ion-neutral interactions. The equatorial number densities are reduced gradually with latitude, with the polar number densities 75% of the equatorial number densities. The temperature at the inner boundary is set to 0.5 eV. The number densities and temperature are held fixed at the inner boundary during the simulations.

[9] The model of the Martian magnetic field was provided by *Cain et al.* [2003]. The magnitude of the anomalous magnetic field at the inner boundary is shown on a 3-D partial sphere in Figures 1 and 4. The simulations were run with the strong southern magnetic anomalies along noon local time and the equatorial plane tilted by 20°. This configuration represents summer solstice in southern hemisphere and the approximate orientation of the planet during the Halloween 2003 superstorm. The x axis points in the direction of the solar wind flow; the z axis is perpendicular to the ecliptic plane and points in the direction of north.

[10] The solar wind is set to nominal conditions with a density of 2 ions cm^{-3} and a speed of 400 km s^{-1}. The Parker spiral approximation of the direction of the IMF at Mars' orbit puts the magnitude of the B_y component 1.5 times larger than the B_x component. Various measurements of solar wind parameters by Phobos 2 and MGS show the magnitude of the IMF in the range of 2-3 nT with the direction in the ecliptic plane primarily in the B_y direction [e.g., *Kallio et al.*, 1995; *Vignes et al.*, 2000]. In the results discussed below, the magnitude of the IMF is equal to 1.2 nT in the $-B_z$ direction. Looking at only a single component allows for less ambiguity regarding the role of reconnection of the southward component of the IMF to the anomalous magnetic on the resulting structures.

[11] The entire simulation encompasses an area from 8 R_M upstream to 36 R_M down tail, and $\pm 17 R_M$ on the flanks and over the poles. The multifluid equations are solved on a nested grid system allowing high resolution around regions of interested. The simulations are first run at coarse resolution until a global equilibrium is achieved (at a time in excess of 10 transit times). Then high-resolution gridding is initiated around the region of interest, in this case the dayside around the magnetic anomalies. The resolution for the results presented in this paper ranges from 1345 km far from the planet, to 42 km in the vicinity of the anomalies on the dayside. For comparison, the ion cyclotron radius for H^+ ranges from 1000 km in the solar wind, to 100 km in the sheath, a few to 10s of km in the MPL, and 0.1 km near the anomalies. The cyclotron radius for O_2^+ ranges from several thousand km in the solar wind, hundreds of km in the sheath, 100 km in the MPL, and a few km in the minimagnetosphere regions. More details about the equations solved and incorporation of ion cyclotron affects can be found in the work of *Winglee* [2004] and *Harnett et al.* [2005].

3. Results

[12] Figure 1 shows several parameters in a plane along the moon meridian. The white dashed curves indicate the location of the bow shock (outermost curve), the magnetic pileup boundary (middle curve), and the ionopause (inner curve) in the northern hemisphere. The curves are determined from the locations of enhanced current density north of approximately 20° and are continued into the southern hemisphere assuming symmetry about the subsolar point. Note that at only 2–3 grid points thick in Figure 1a, the

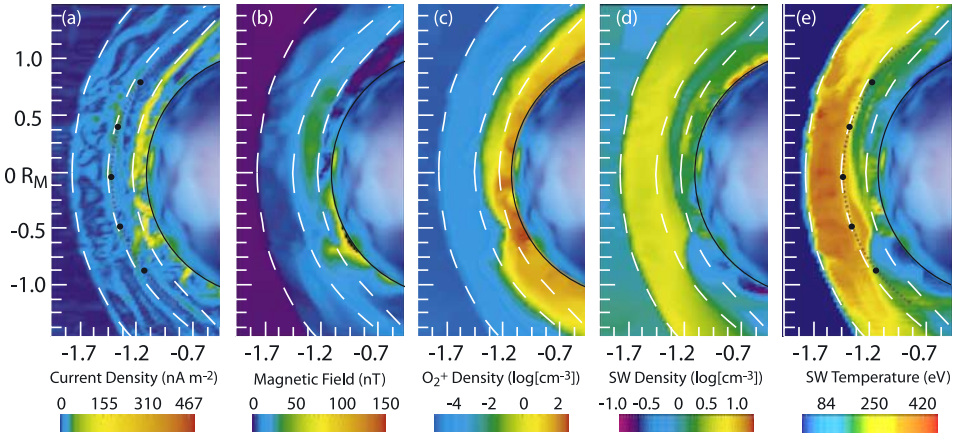

Figure 1. The (a) current density, (b) magnetic field magnitude, (c) oxygen density, (d) solar wind density, and (e) solar wind temperature in the plane through the noon meridian.

thickness of the boundaries in the northern hemisphere is not fully resolved. A map of the magnetic field strength of the anomalies at the inner boundary is also shown, with a black curve indicating the edge of the inner boundary in the plane shown. Also shown in Figures 1a and 1e are purple spheres at the locations the data is sampled at when at a constant altitude of 1360 km. The trajectory starts in the northern hemisphere at 55° and ends in the southern hemisphere at −55°. There are 60 sample locations in total and every 10th location is indicated with a larger black circle. The resolution of the area shown ranges between 84 km at the edges of the area shown, to 42 km around the anomalies.

[13] For nominal solar wind conditions, the subsolar point of the bow shock forms at approximately 1.7 R_M (Figure 1), in agreement with the average location calculated by *Vignes et al.* [2000]. Inside the bow shock, a high-temperature sheath regions forms (Figure 1e). At the inner edge of the sheath, in the northern hemisphere northward of approximately 20°N, the current density and magnetic field increase (Figures 1a and 1b). At the same location, the solar wind density and temperature decrease (Figures 1d and 1e). These are indicators of a standard magnetic pileup boundary (MPB). The current density at the MPB is approximately 60 nA m^{-2}, comparable to the value of 80 nA m^{-2} estimated by *Bertucci et al.* [2005] from MGS data.

[14] The subsolar distance for a curve fit to the MPB in the northern hemisphere is approximately 1.45 R_M. This is 0.15 R_M (or six grid points) further away than the average position calculated calculated from MSG observations by *Vignes et al.* [2000] and 0.05 R_M (or two grid points) further away than the average position calculated, also from MSG observations, by *Crider et al.* [2002]. Owing to the thickness of the boundary at the subsolar point, the MPB subsolar position in the simulations is based on a curve fit to the MPB in the northern hemisphere. When accounting for this uncertainty, the simulation MPB subsolar distance is in agreement with the value determined by *Crider et al.* [2002] but further from the planet than the value determined by *Vignes et al.* [2000].

[15] The simulations also show a current boundary in the southern hemisphere, indicative of an MPB, forming at approximately the same altitude as the MPB in the northern hemisphere (Figure 1a). *Brain et al.* [2005] found that at the southern hemisphere summer solstice, MGS measurements showed that the MPB moved further away from the planet on the entire dayside, not just over the anomalies. However, MGS was in a circular orbit at ∼400 km during the time period that the data was analyzed so they were not able to quantify how far the MPB moved away from the planet. The model results confirm this measurement of a global affect on the MPB by the anomalous magnetic field. The altitude of the MPB at higher latitudes is closer than the ∼1.56 R_M that *Crider et al.* [2002] determined for the average MPB location at 30°S.

[16] The MPB forms the outer boundary of the magnetic pileup layer (MPL). The current density (Figure 1a) in the northern hemisphere indicates the model is resolving another boundary at the inner edge MPL. Inside this boundary the magnetic field (Figure 1b) decreases sharply while both the O_2^+ (Figure 1c) and ionospheric H^+ density increases, indicating that the boundary is the ionopause. In the southern hemisphere, the region inside of the MPB has more structure than that of a smooth transition to an ionopause due to the anomalous magnetic field.

[17] Just inside the MPB in the southern hemisphere, the magnetic field magnitude increases, indicative of an MPL. While the peak magnetic field in the MPL in the northern hemisphere is 30–40 nT, the magnetic field in this MPL-like boundary in the southern hemisphere is ∼20 nT (Figure 1b). A further difference between this MPL-like region in the southern hemisphere and the MPL in the northern hemisphere appears when comparing the ionospheric oxygen density (Figure 1c), the solar wind density (Figure 1d), ionospheric hydrogen density, and electron density between the two hemispheres. These parameters indicate the MPL-like region in the southern hemisphere is populated by more ionospheric plasma and less solar wind plasma than the MPL region in the northern hemisphere.

[18] Figure 2 shows the ion and electron densities at two altitudes within the MPL/MPL-like regions. The values are sampled along two constant altitude trajectories beginning in the northern hemisphere at a latitude of 55° and ending in the southern hemisphere at a latitude of −55°. For the region sampled, the trajectories in the northern hemisphere are in the MPL between 55° and 30° and in the the MPL-like region in the southern hemisphere between

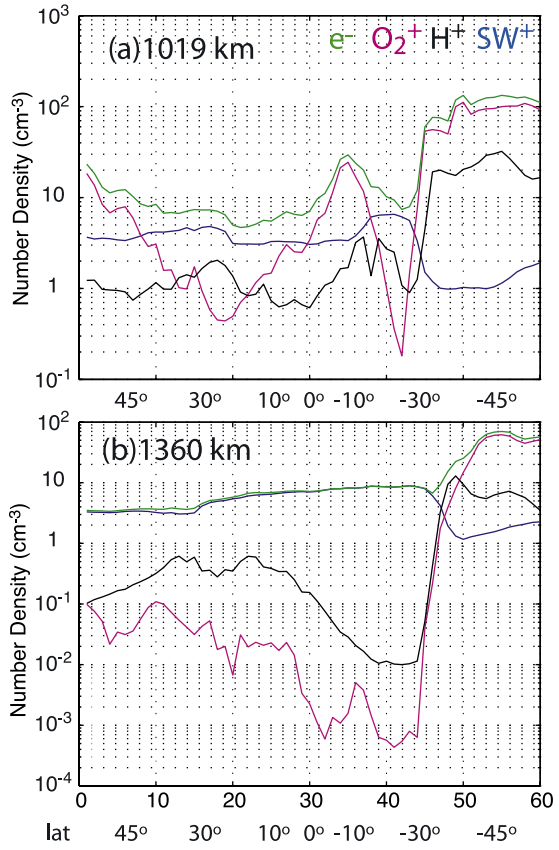

Figure 2. Number density of ionospheric O_2^+ (magenta), ionospheric H^+ (black), solar wind H^+ (blue) and electrons (green) at constant altitudes of (a) 1019 km and (b) 1360 km. The values at 1360 km are sampled at the locations shown in Figures 1a and 1e. Both the sample location and latitude are given along the x axis.

approximately −30° and −55°. At ∼ ±50° the solar wind density is approximately constant with altitude between 1000 km and 1400 km at 3–4 cm^{-3} in the northern hemisphere and 1 − −2cm^{-3} in the southern hemisphere.

[19] The ionospheric ion densities do decrease with increasing altitude but with different scaling for either species. At +55° the H^+ density decreases by a factor of 10, from 1.0 cm^{-3} at 1019 km to 0.1 cm^{-3} at 1360 km, while the O_2^+ density decreases by a factor of 200 from 20.0 cm^{-3} at 1019 km to 0.1 cm^{-3} at 1360 km. This would indicate scale heights of 150 km for H^+ and 75 km for O_2^+. Below the ionopause (at ∼500 km, and ∼ +50°), the density falloff translates to a scale height of approximately 130 km for H^+ and 220 km for O_2^+. In the southern hemisphere the anomalies protect the ionosphere from the solar wind. There is less solar wind present and significantly more ionospheric ions. The ionospheric densities in the high-latitude regions are 10–600 times larger than the densities at corresponding latitudes in the northern hemisphere. At −55°, the H^+ density is 20 cm^{-3} at 1019 km, while the O_2^+ density is 100 cm^{-3}, both ∼10 times larger than at the same latitude in the northern hemisphere. At 1360 km, the densities of H^+ and O_2^+ are 50 to 600 times larger than at the same latitude in the northern hemisphere, at 5.0 cm^{-3} and 60.0 cm^{-3}, respectively. This density decrease corresponds to scale heights of 250 km for H^+ and 670 km for O_2^+. Thus in addition to more plasma being present, the scale height in the southern hemisphere is typically larger than in the northern hemisphere. At ∼500 km and ∼ −50°, the density falloff indicates a scale height of approximately 280 km for H^+ and 904 km for O_2^+. Note that these scale heights would invariably be altered by the inclusion of collisions and interactions with neutrals, which are not accounted for in these simulations.

[20] Further comparison between the northern and southern hemisphere can be made by looking at spectrograms along one of the trajectories. The results in Figure 3 are sampled along a constant altitude of 1360 km. At the beginning of the trajectory, the synthetic spacecraft is in the MPL. At a latitude of approximately 35° (or position 12), the spacecraft crosses into the MPB, as seen by an increase in the current density (Figure 3e). Associated with this region is a decrease in the energy of ionospheric ions (Figures 3b and 3c) and an increase in the energy of the solar wind (Figure 3d) and the electrons (Figure 3a). The spacecraft remains in the MPB until a latitude of 5° where the current density decreases and it enters the sheath (SH). In this regions, the flux of oxygen disappears and the flux of ionospheric hydrogen decreases. The flux of ionospheric hydrogen does not completely disappear because it is not gravitationally bound to the planet.

[21] Comparison of the electron spectrogram to measurements made by MGS as it traversed the MPB, MPL and possibly the ionopause, as shown by *Vignes et al.* [2002], indicates that the simulation results are consistent with MGS measurements. *Vignes et al.* [2002] state that one characteristic used to identify the MPB crossings is a reduction in electron flux at energies greater than 10 eV. In the simulations, crossing from the MPB into the MPL (i.e., moving from 25° to 35° in Figure 3a), the electron spectrum shifts to lower energy, with approximately an order of magnitude decrease in the flux at a given energy above 10 eV. For example, the flux of 100 eV electrons in the MPB is $\sim 10^2$ cm^{-2} s^{-1} eV^{-1}, while in the MPL, the flux of 100 eV electrons is ∼10 $cm^{-2}s^{-1}$ eV^{-1}. Note that the model assumes Maxwellian distributions and thus the model electron spectrograms do not contain the high energy tail component that is present in the data. Peak electron fluxes outside of the ionosphere are on the order of $10^6 - 10^7$ cm^{-2} $s^{-1}eV^{-1}$, consistent with measurements shown by *Mitchell et al.* [2001].

[22] At about −5°, the spacecraft enters a region where the current density increases, indicating another boundary (C). Looking at the region in the highest resolution (Figure 4) we can see that the C region is along draped IMF that connect to the surface (Figure 4b). At the foot of the open field lines, the solar wind density reaches 10 cm^{-3} and 420 eV, equivalent to the solar wind temperature in the sheath. A moderate increase in the flux of oxygen also occurs in this regions. Thus region C is defined as a cusp. It also forms the boundary between the region to the north of reduced solar wind and cold dense ionospheric plasma, and the hot, solar wind-rich plasma to the south. The sheath-like energy spectrum of electrons has been used to identify cusps in MEX data [*Soobiah et al.*, 2006; *Franz et al.*, 2006] and in MGS data in conjunction with measurements of mostly radial magnetic field [*Mitchell et al.*, 2001; *Brain et al.*, 2005].

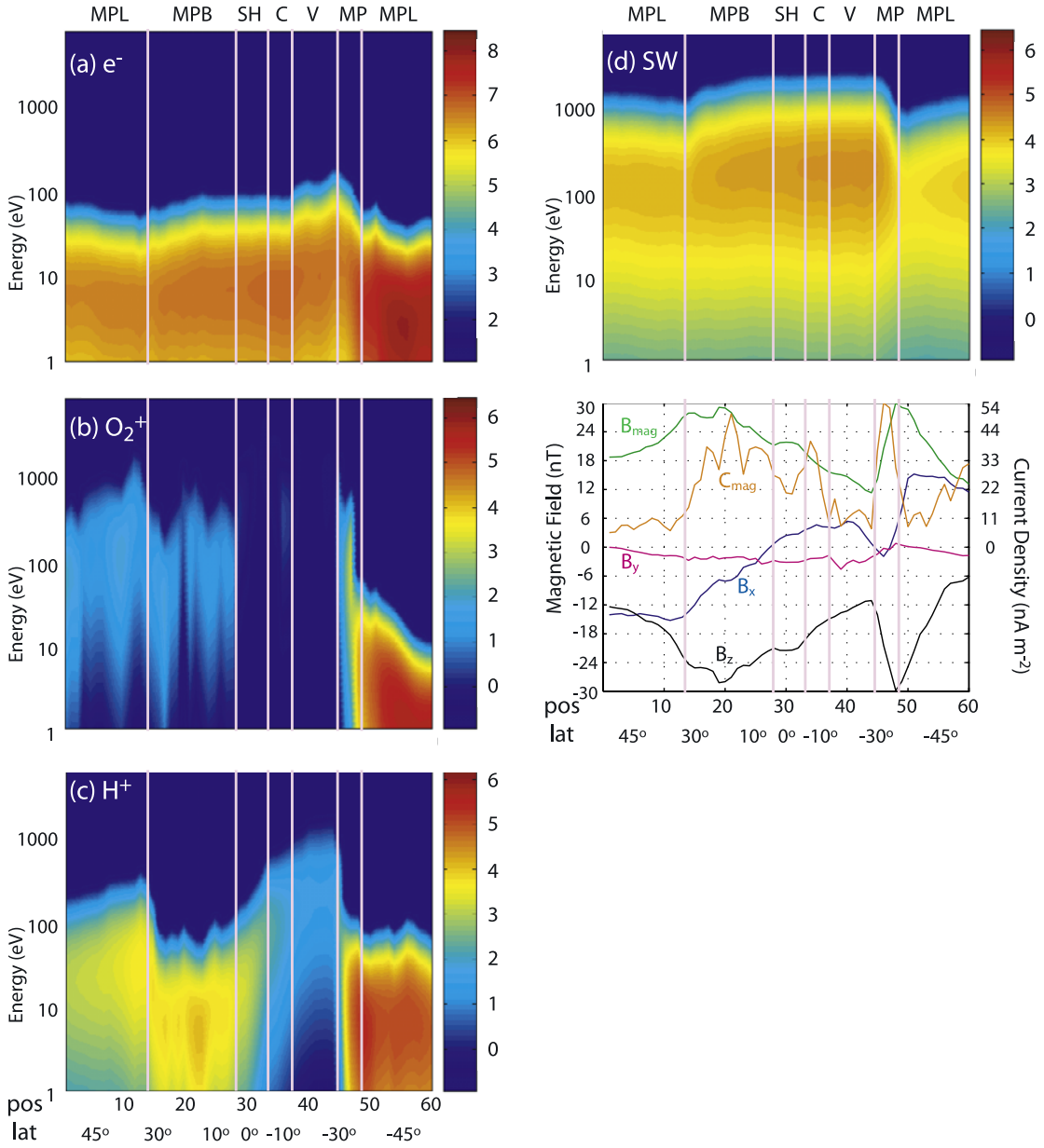

Figure 3. Spectrograms for (a) electrons, (b) ionospheric O_2^+, (c) ionospheric H^+, and (d) solar wind H^+, as well as magnetic field and current density traces, generated from simulation data at each sample location shown in Figures 1a at a constant altitude of 1360 km. Both the sample location and latitude are given along the x axis. The flux is in units of $cm^{-2}\ s^{-1}\ eV^{-1}$. Also shown is (e) the magnitude of all three magnetic field components and the total magnitude (B_x, B_y, B_z, B_{mag}) as well as the magnitude of the current density (C_{mag}) along the trajectory. Boundary crossings are indicated with vertical lines. See text for definitions.

[23] At −10° the spacecraft exits the cusp, as seen by a decrease in the current density. The oxygen and solar wind spectra (Figures 3b and 3d) remain sheath-like in this region (V). The electron energy increases slightly while the energy of ionospheric hydrogen is approximately an order of magnitude larger than in the previous sheath region (SH) (Figure 3a and 3c). The ionosphere is significantly eroded in this sheath-like region southward of the cusp (∼−20° or in the lower portion of Figures 4c and 4d), with ionospheric densities 100 times less dense than the same altitude in the northern hemisphere. The magnetic field magnitude is reduced by 40–50% to only 12 nT in this region as well (Figure 1b). The magnetic field geometry (Figure 4b) suggests that this is a region undergoing continuous reconnection. As a result, the ionosphere is eroded and a void (V) region forms. This type of void is different from those seen by *Mitchell et al.* [2001]. This void region is on the dayside and has low density at the result of continuous reconnection to the IMF. The voids seen by *Mitchell et al.* [2001] formed on the nightside and were regions protected from planetward plasma flows by the anomalous magnetic field. There is one similarity

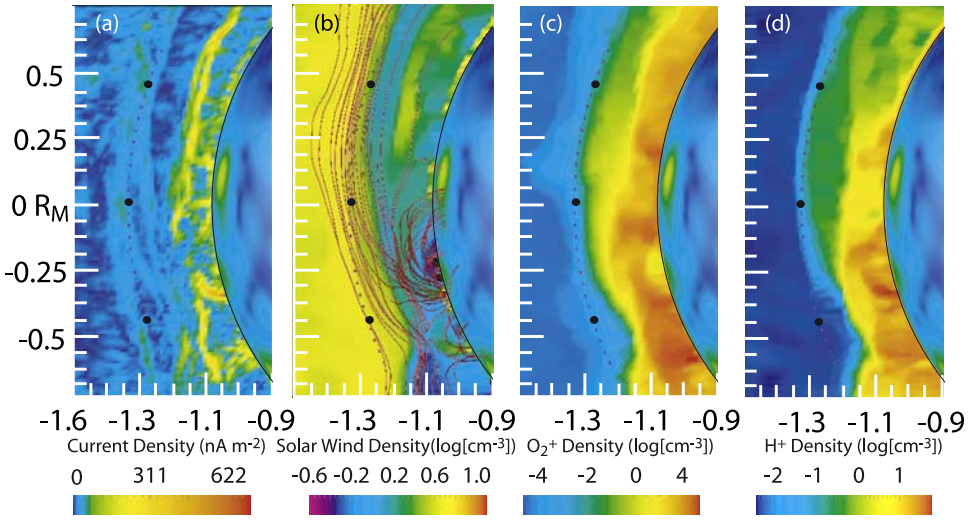

Figure 4. Highest resolution images of (a) current density, (b) solar wind H^+ density and magnetic fieldlines, (c) ionospheric O_2^+ density, and (d) ionospheric H^+ density in the same plane as the images in Figure 1. The resolution is 42 km in all of the area shown. The spacecraft sample positions in this region are also shown and range from 25° to −25°. The black circles indicate positions 20, 30, and 40.

between the two cases though in the magnetic field and plasma properties adjacent to the voids. In both cases (dayside void in the simulations, and nightside voids in MGS data), the magnetic field and electron spectra suggest the regions just outside of the voids are on open magnetic field line and the plasma is of shocked-solar wind origin.

[24] After the void region (V), at a latitude of about −30°, the spacecraft crosses into a region where the flux of the ionospheric components increases by several orders of magnitude while the temperature decreases. At the boundary the magnetic field undergoes large changes with B_x and B_y approaching zero, while B_z goes strongly negative (Figure 3e). This indicates a region transitioning from magnetic fields of solar wind origin (both IMF and induced) to a region dominated by anomalous magnetic field and suggests that the boundary is a magnetopause (MP). A magnetopause can form because the B_z component of the anomalous magnetic field is aligned with the IMF in this region, instead of being antialigned, as in the void region to the north. The region inside the MP boundary is ionospheric-like in that the the large flux of ions is also cold (Figures 3b–3c), and while the solar wind flux is reduced, it does not completely disappear (Figure 3d).

[25] The constant altitude pass highlights the difference between the northern and southern hemispheric plasma populations but it leaves some ambiguity with regarding the nature of all the boundaries seen in Figures 1–4 because it crosses the boundaries obliquely. To resolve the exact nature of the boundaries one has to look at the whole picture, and multiple spectrograms, not just a single 1-D cut through the results. When that is done, a picture illustrated by Figures 5a and 5b emerges. To highlight the difference between the MPB/MPL region in the northern and southern hemisphere and the MPB verses a magnetopause boundary, magnetic field traces along straight line cuts are also shown (Figures 5c–5e).

[26] In the northern hemisphere (Figure 5c), the magnetic field magnitude behaves according to the conventional picture [e.g., *Bertucci et al.*, 2005]. The magnetic field magnitude begins to increase at the bow shock and then plateaus in the sheath (Figure 5a). At the MPB, a further increase in the magnetic field magnitude occurs, with the maximum values occurring at the inner edge of the MPL. The thickness of the MPL is on the order of 600 km, as measured radially. Depending on where the MPL is traversed in the northern hemisphere, peak magnetic field strengths range between 20 nT and 40 nT, consistent with values measured by MGS [e.g., *Vignes et al.*, 2000]. The model can not show the high-frequency waves present in the magnetic field data external to the MPL. The ionopause demarcates the inner edge of the MPL, across which the magnetic field rapidly decreases. There is only nominal magnetic field inside induced by the currents in the ionosphere.

[27] In the void region the structure deviates from this picture. The boundary just south of the void region is a magnetopause, and neither an MPB/MPL nor an ionopause is present in the void region or just to the south. Reconnection of the IMF to the anomalous magnetic field means the IMF cannot pile up, thus and MPB does not form. The subsequent erosion of the ionosphere by the solar wind means there is insufficient plasma for the formation of an ionopause either. The dominate source of pressure in inhibiting solar wind access is the anomalous magnetic field. This region, marked MP in Figure 5b, is classified as a magnetopause instead of an MPB because the anomalous magnetic field accounts for nearly 50% of the total magnetic field at this boundary (Figure 5d). In contrast, in the MPL both to the north and to the south, the anomalous magnetic field makes up only ∼20% of the total magnetic field. Also inside the magnetopause, the solar wind density and temperature are smaller than at any location inside the bow shock in the northern hemisphere including inside the ionopause (Figures 1d and 1e). The boundary forms as a result of magnetic field of planetary origin thus is defined as a magnetopause.

[28] Further south, the ionosphere is not eroded and an MPB/MPL are present but in this region a magnetopause forms at the inner edge of the MPL due to the presence of the anomalous magnetic field. The magnetic field trace initially looks similar to that in the northern hemisphere, with an initial rise in the magnetic field strength at the bow shock (Figure 5e) and a further increase at the MPB. The magnetic field reaches a local maximum at the inner edge of the MPL and decreases further inside. At the location of maximum magnetic field in the MPL the anomalous magnetic field is still only 24% of the total, and while the total magnetic field decreases closer to the surface, the anomalous magnetic field continues to increase (Figure 5e). At the outer edge of the magnetopause, B_y changes sign and the solar wind velocity becomes small. However, it is not until the inner edge of the magnetopause that \text{B}_z goes to zero and the solar wind density and temperature become very small, the smallest for the entire dayside area shown in Figure 1 and even smaller than inside the magnetopause to the north.

[29] A second cusp forms in the southern hemisphere (Figures 5a–5b) where the anomalous magnetic field has a large $+B_z$ component, like the cusp to the north. The solar wind has enhanced access to the surface in this region. However, the fact that this cusp forms inside the MPB means that while the solar wind density and temperature are enhanced at the footpoint at the surface, they are not as large as at the footpoint of the cusp to the north.

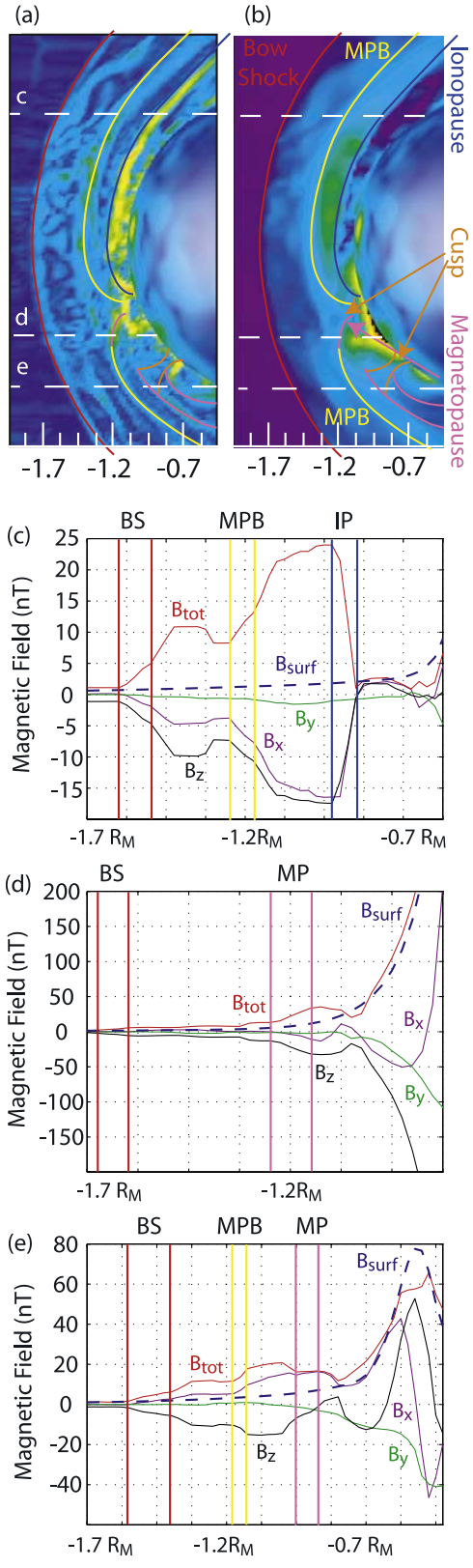

4. Conclusions

[30] High-resolution multifluid simulations of the solar wind interaction with Mars indicate that the anomalous magnetic field can have a global effect on the magnetosphere during the southern hemisphere summer solstice. The results agree with MGS data indicating that for this orientation the anomalies push the MPB away from the surface over the entire dayside, not just around the anomalies [*Brain et al.*, 2005]. The simulations also indicate that the anomalous magnetic field modifies the characteristics of the MPB and MPL relative to over unmagnetized regions. Spectrograms taken at a constant altitude suggest that the inner edge of the MPL forms below 1360 km in the northern hemisphere, but above 1360 km in the southern hemisphere, as the spectrograms indicate a cool, dense plasma, more ionospheric in nature at 1360 km in the southern hemisphere. Further analysis by looking at not only the magnetic field along a single trajectory but also different plasma parameters in the general area, indicates otherwise. The MPL does not terminate above 1360 km in the southern hemisphere but rather the presence of the anomalous magnetic field leads to higher ion densities than in the MPL in the northern hemisphere. The anomalous magnetic field also leads to the formation of magnetopause boundary at the inner edge of the MPL, instead of the ionopause that forms

Figure 5. The (a) current density and (b) magnetic field magnitude (same as Figures 1a and 1b) with boundary identification marked. The magnetic field plots (c–e) are for straight line cuts along the white dotted lines in Figures 5a and 5b. The quantities shown are the total magnetic field components (B_x, B_y, B_y), the total magnetic field magnitude (B_{mag}), and the magnitude of the the anomalous magnetic field only (B_{surf}). The boundaries are identified with vertical bars the same color as the traces in the images and by the following: BS = bow shock, MPB = magnetic pileup boundary, IP = ionopause, and MP = magnetopause.

over unmagnetized regions. The results suggest that spectrograms alone may not be able to unambiguously determine when a satellite traverses different boundaries. In the simulation results some boundaries are more evident in one species than another, with the magnetic field resolving the ambiguities.

[31] The next step in the simulations will be to modify the solar wind conditions such that they better represent the possible conditions at Mars during the 2003 Halloween superstorm [*Skoug et al.*, 2004]. No satellites were in the position to monitor the solar wind conditions at Mars during the event and therefore the conditions need to be estimated from those measured at the Earth and from proxies determined from measurements made within the magnetosphere [e.g., *Crider et al.*, 2003]. *Crider et al.* [2005] found that the magnetosphere of Mars was highly compressed during the event, suggesting increased mass loss occurred, as the solar wind had access to much lower altitudes than during nominal conditions. The high speeds of the solar wind and strong magnetic field strengths of the IMF means the solar wind conditions during the 2003 Halloween superstorm are analogous to the most likely nominal conditions for the early Sun [e.g., *Harnett and Winglee*, 2006]. This makes the event a good case to use as an early Sun proxy when trying to validate model predictions of ionospheric loss due to solar wind interactions early in Martian history.

[32] **Acknowledgments.** This research was supported by NASA grant NAG 5-11869.

[33] Wolfgang Baumjohann thanks the reviewers for their assistance in evaluating this paper.

References

Acuna, M. H., et al. (1999), Global Distribution of Crustal Magnetization Discovered by the Mars Global Surveyor MAG/ER Experiment, *Science*, *284*, 790–793.

Bertucci, C., et al. (2005), Structure of the magnetic pileup boundary at Mars and Venus, *J. Geophys. Res.*, *110*, A01209, doi: 10.1029/2004JA010592.

Brain, D. A., et al. (2005), Variability of the altitude of the Martian sheath, *Geophys. Res. Lett.*, *32*, L18203, doi:10.1029/2005GL023126.

Cain, J. C., et al. (2003), An n = 90 internal potential function of the Martian crustal magnetic field, *J. Geophys. Res.*, *108*(E2), 5008, doi:10.1029/2000JE001487.

Connerney, J. E. P., et al. (1999), Magnetic Lineations in the Ancient Crust of Mars, *Science*, *284*, 794–798.

Crider, D. H., et al. (2000), Evidence of electron impact ionization in the magnetic pileup boundary of Mars, *Geophys. Res. Lett.*, *27*, 45–48.

Crider, D. H., et al. (2002), Observations of the latitude dependence of the location of the Martian magnetic pileup boundary, *Geophys. Res. Lett.*, *29*(8), 1170, doi:10.1029/2001GL013860.

Crider, D. H., et al. (2003), A proxy for determining solar wind dynamic pressure at Mars using Mars Global Surveyor data, *J. Geophys. Res.*, *108*(A12), 1461, doi:10.1029/2003JA009875.

Crider, D. H., et al. (2005), Mars Global Surveyor observations of the Halloween 2003 solar superstorm's encounter with Mars, *J. Geophys. Res.*, *110*, A09S21, doi:10.1029/2004JA010881.

Franz, M., et al. (2006), Plasma intrusion above Mars crustal fields-Mars Express ASPERA-3 observations, *Icarus*, *182*, 406–412.

Hanson, W. B., et al. (1977), The Martian ionosphere as observed by the Viking retarding potential analyzers, *J. Geophys. Res.*, *82*, 4351–4363.

Harnett, E. M., and R. M. Winglee (2003), The influence of a mini-magnetopause on the magnetic pileup boundary at Mars, *Geophys. Res. Lett.*, *30*(20), 2074, doi:10.1029/2003GL017852.

Harnett, E. M., and R. M. Winglee (2006), Three-dimensional multifluid simulations of ionospheric loss at Mars from nominal solar wind conditions to magnetic cloud events, *J. Geophys. Res.*, *111*, A09213, doi:10.1029/2006JA011724.

Harnett, E. M., et al. (2005), Pluto's magnetosphere: A comparison between 3D hybrid and 3D multi-fluid simulation results, *Geophys. Res. Lett.*, *32*, L19104, doi:10.1029/2005GL023178.

Kallio, E., et al. (1995), Oxygen outflow in the Martian magnetotail, *Geophys. Res. Lett.*, *22*, 2449–2453.

Lundin, R., et al. (2004), Solar wind-induced atmospheric erosion at Mars: First results from ASPERA-3 on Mars Express, *Science*, *305*, 1933–1936.

Lundin, R., et al. (2006), Ionospheric plasma acceleration at Mars: ASPERA-3 results, *Icarus*, *182*, 308–319.

Ma, Y., et al. (2002), Three-dimensional multispecies MHD studies of the solar wind interaction with Mars in the presence of crustal fields, *J. Geophys. Res.*, *107*(A10), 1282, doi:10.1029/2002JA009293.

Mazelle, C., et al. (1989), Analysis of suprathermal electron properties at the magnetic pileup boundary at Comet P/Halley, *Geophys. Res. Lett.*, *16*, 1035–1038.

Mitchell, D. L., et al. (2001), Probing Mars' crustal magnetic field and ionosphere with the MGS electron reflectometer, *J. Geophys. Res.*, *106*, 23,418–23,427.

Riedler, W. D., et al. (1989), Magnetic field near Mars, *Nature*, *341*, 604–607.

Skoug, R. M., et al. (2004), Extremely high speed solar wind: 29–30 October 2003, *J. Geophys. Res.*, *109*, A09102, doi:10.1029/2004JA010494.

Soobiah, Y., et al. (2006), Observations of magnetic anomaly signatures in Mars Express ASPERA-3 ELS data, *Icarus*, *182*, 396–405.

Vignes, D., et al. (2000), The solar wind interaction with Mars: locations and shapes for the bow shock and the magnetic pile-up boundary from the observations of the MAG/ER experiment onboard Mars Global Surveyor, *Geophys. Res. Lett.*, *27*, 49–52.

Vignes, D., et al. (2002), Factors controlling the location of the Bow Shock at Mars, *Geophys. Res. Lett.*, *29*(9), 1328, doi:10.1029/2001GL014513.

Winglee, R. M. (2004), Ion cyclotron and heavy ion effects on reconnection in a global magnetotail, *J. Geophys. Res.*, *109*, A09206, doi: 10.1029/2004JA010385.

E. M. Harnett and R. M. Winglee, Department of Earth and Space Science, Box 351310, University of Washington, Seattle, WA 98195-1310, USA. (eharnett@ess.washington.edu; winglee@ess.washington.edu)